PAPER

Proton-fluence dependent magnetic properties of exfoliable quasi-2D van der Waals ${\rm Cr_2Si_2Te_6}$ magnet

To cite this article: Hector Iturriaga et al 2024 J. Phys.: Condens. Matter 36 225801

View the article online for updates and enhancements.

You may also like

- Rotational phase transitions in antifluoritetype osmate and iridate compounds
 A Bertin, L Kiefer, P Becker et al.
- Identification of paramagnetic centers in irradiated Sn-doped silicon dioxide by firstprinciples
- L Giacomazzi, L Martin-Samos, N Richard et al
- Linear response theories for interatomic exchange interactions

Proton-fluence dependent magnetic properties of exfoliable quasi-2D van der Waals Cr₂Si₂Te₆ magnet

Hector Iturriaga^{1,9}, Ju Chen^{2,9}, Jing Yang², Luis M Martinez^{1,3}, Lin Shao⁶, Yu Liu^{7,8}, Cedomir Petrovic⁷, Martin Kirk^{2,4,5,*} and Srinivasa R Singamaneni^{1,*}

E-mail: mkirk@unm.edu and srao@utep.edu

Received 19 November 2023, revised 23 January 2024 Accepted for publication 9 February 2024 Published 5 March 2024



Abstract

The discovery of long-range magnetic ordering in atomically thin materials catapulted the van der Waals (vdW) family of compounds into an unprecedented popularity, leading to potentially important technological applications in magnetic storage and magneto-transport devices, as well as photoelectric sensors. With the potential for the use of vdW materials in space exploration technologies it is critical to understand how the properties of such materials are affected by ionizing proton irradiation. Owing to their robust intra-layer stability and sensitivity to external perturbations, these materials also provide excellent opportunities for studying proton irradiation as a non-destructive tool for controlling their magnetic properties. Specifically, the exfoliable $Cr_2Si_2Te_6$ (CST) is a ferromagnetic semiconductor with the Curie temperature (T_C) of \sim 32 K. Here, we have investigated the magnetic properties of CST upon proton irradiation as a function of fluence $(1 \times 10^{15}, 5 \times 10^{15}, 1 \times 10^{16}, 5 \times 10^{16}, \text{ and } 1 \times 10^{18} \text{ H}^+/\text{cm}^{-2})$ by employing variable-temperature, variable-field magnetization measurements, and detail how the magnetization, magnetic anisotropy vary as a function of proton fluence across the magnetic phase transition. While the $T_{\rm C}$ remains constant as a function of proton fluence, we observed that the saturation magnetization and magnetic anisotropy diverge at the proton fluence of $5 \times 10^{16} \,\mathrm{H^+/cm^{-2}}$, which is prominent in the ferromagnetic phase, in particular.

© 2024 IOP Publishing Ltd

¹ Department of Physics, The University of Texas at El Paso, El Paso, TX 79968, United States of America

² Department of Chemistry and Chemical Biology, The University of New Mexico, MSC03 2060, 1 University of New Mexico, Albuquerque, NM 87131-0001, United States of America

³ Center for Integrated Nanotechnologies, Los Alamos National Laboratory, Los Alamos, NM 87545, United States of America

⁴ The Center for High Technology Materials, The University of New Mexico, Albuquerque, NM 87106, United States of America

⁵ Center for Quantum Information and Control (CQuIC), The University of New Mexico, Albuquerque, NM 87131-0001, United States of America

⁶ Department of Nuclear Engineering, Texas A&M University, College Station, TX 77845, United States of America

⁷ Condensed Matter Physics and Materials Science Department, Brookhaven National Laboratory, Upton, NY 11973, United States of America

Present address: Center for Correlated Matter and School of Physics, Zhejiang University, Hangzhou 310058, People's Republic of China

⁹ Equally contributed.

Authors to whom any correspondence should be addressed.

This work demonstrates that proton irradiation is a feasible method for modifying the magnetic properties and local magnetic interactions of vdWs crystals, which represents a significant step forward in the design of future spintronic and magneto-electronic applications.

Supplementary material for this article is available online

Keywords: van der Waals magnets, proton irradiation, magnetism

1. Introduction and motivation

Pioneering transition metal-based vdW magnets such as CrI₃ and Cr₂Ge₂Te₆ have been successfully studied at the singlelayer limit, displaying novel and exciting long-range magnetic ordering at the 2-dimensional level. This provides the impetus for the creation of ultrathin magnetic data storage devices, spintronic applications, and other cost-effective magnetic devices [1–5]. Of particular importance, with the current interest in space exploration technologies, it is beneficial to investigate the behavior of these materials under the effects of proton irradiation. In space, where proton irradiation is abundant, bombardment by such particles can quickly modify their electronic and magnetic properties. Thus, the robust intralayer properties of these compounds make them excellent candidates for studying the limits of proton irradiation on technologically relevant properties of such functional materials. Particularly, though not exclusively, in the case of ternary transition metal-based vdW chalcogenides such as Fe_{2.7}GeTe₂ (FGT) and Mn₃Si₂Te₆ (MST), our group and others have found that proton irradiation serves as a nondestructive tool for controlling the magnetic properties of these compounds [6-11]. These compounds owe their enhanced magnetization after irradiation to their strong intralayer bonding, robust magnetic character, and their sensitivity to external perturbations.

Here, we explore the effects of non-destructive proton irradiation on the related compound Cr₂Si₂Te₆ (CST). Paired with its layer-dependent magnetism, studies on proton-irradiated CST may facilitate new discoveries and breakthroughs in the creation of functional 2D magnets, novel heterostructures, and new high-speed magnetic devices [12-14]. Although the ferromagnetic ordering temperature is only 32 K in this ternary chromium chalcogenide, making it unsuitable for consumer applications, its magnetic properties are stable under extreme conditions leading to potential roles for these materials in space exploration technology applications [15– 17]. As such, proton irradiation may provide an attractive approach to enhance the properties of CST without destroying the material. For this reason, we have investigated the evolution of the Curie temperature $(T_{\rm C})$, saturation magnetization, and magnetocrystalline anisotropy in CST crystals that have been irradiated with proton doses of up $1 \times 10^{18} (H^{+})/cm^{-2}$ by employing variable-temperature, variable-field magnetization measurements coupled with Raman and electron paramagnetic resonance (EPR) spectroscopy.

2. Experimental details

The synthesis of mm-sized CST crystals was conducted as previously reported with the self-flux method starting with Cr powder and Si and Te pieces [18]. The crystals were then irradiated with a 2 MeV proton beam in 1.7 MV Tandetron Accelerator following closely the procedure discussed in [6– 9]. The energy of the beam is kept low enough to avoid damage to the crystal. In addition, the weak beam current of 100 nA, beam spot size of 6 mm × 6 mm rastered over an area of $1.2 \text{ cm} \times 1.2 \text{ cm}$, and magnetic bending filters ensure lateral beam uniformity, minimal heating, and eliminate carbon contamination. The projected implantation depth is approximately 35 μ ms according to the damage profile, which shows a uniform distribution of H from the surface down to approximately 30 μ ms from the surface. The fluences selected for this study are 0 (referred to as pristine in this work), 1×10^{15} , 5×10^{15} , 1×10^{16} , 5×10^{16} , and 1×10^{18} H⁺/cm⁻².

The magnetic properties of the crystals were characterized using a Quantum Design Magnetic Property Measurement System 3 (MPMS 3) Superconducting QUantum Interference Device/Vibrating Sample Magnetometer (SQUID/VSM) hybrid system. DC magnetic moment data were extracted using the VSM option throughout all temperature and field ranges. The measurements were conducted in a temperature range of 2 K-300 K and at magnetic fields up to 30 kOe in both polarities. Samples were loaded separately into the MPMS by wrapping them in Teflon tape to avoid contamination from sample holders or from contact with the instrument chamber. In the case of magnetic moment anisotropy measurements, we used both quartz and brass sample holders, which allow for in-plane (where the crystallographic ab-plane is parallel to the applied field) and out-of-plane (where the c-axis is parallel to the applied field) magnetization measurements. Contributions to the magnetic moment from the sample holders were corrected using the MPMS 3 MultiVu software. The brass sample holder does not have an appreciable magnetization response moving through the SQUID detection coils due to the fact the sample holder length is markedly longer than the scan length through the pickup coils by about a factor of 5.

Temperature-dependent X-band (\sim 9.49 GHz) EPR spectroscopic studies were also performed for each sample. Samples were individually wrapped with Teflon tape and mounted onto a sample holder assembly such that the c-axis of the crystal was oriented parallel to the applied magnetic field. Measurements were performed by first setting the temperature

and allowing the samples to reach thermal equilibrium, and then the scanning the magnetic field between 0 G and 7000 G. To avoid the effects of remanent magnetization between temperature points, the magnetic field was removed, the sample was warmed above its Curie temperature, and finally cooled down to the next temperature point. Measurements were performed at select temperatures between 10 K and 77 K. Raman spectra were collected in parallel geometry using a Renishaw Raman spectrometer using 532 nm laser wavelength excitation with 15 s count and a 50x optical microscope objective.

3. Results and discussion

The Raman spectra (see, figure S1, supplemental information) measured on all the samples indicate that the crystalline structure remains unchanged upon proton irradiation. Figure 1(a) shows a plot of magnetization vs. temperature at various proton fluences. The data were collected along the out-of-plane (H//c) direction with a cooling field of 1 kOe. These field cooled (FC) measurements were conducted by cooling the sample from room temperature down to 10 K under an applied magnetic field. The sample was then allowed to reach thermal equilibrium before the magnetic field was set to 500 Oe, and then the temperature was increased incrementally back to 300 K. For a better visualization of the ferromagnetic phase of CST, only the range from 10 K-100 K is shown in figure 1, since the samples are paramagnetic beyond 50 K. As reflected in this figure, a sharp ferromagnetic to paramagnetic transition is noticed for all the samples regardless of proton fluence. Estimation of the Curie temperature (T_C) via the first derivative of the magnetization with respect to the temperature (figure 1(b)) yields a value of approximately 36 K, which agrees well with literature reports [18-25]. In addition, the low temperature behavior shows that there is a clear change in magnetization after irradiation. The magnetization of the $5 \times 10^{15} \text{ H}^+/\text{cm}^{-2}$ fluence (orange, upright triangles) slightly exceeds the magnetization of the pristine sample at 10 K, before rapidly dropping below the magnetization of the pristine sample at 12 K. For all other proton fluences, we observed a clear decrease in the magnetization. We believe that there is a small Curie-Weiss component induced by the proton irradiation as all the magnetization curves below $T_{\rm C}$ display an upward turn at lowest temperatures (see, appendix in supplemental information). These deviations in the irradiated samples relative to the pristine material are also clearly evident in the dM/dT plot (figure 1(b)).

We note that at 10 K, the proton irradiated sample with a $5 \times 10^{16}~\rm H^+/cm^{-2}$ fluence (figure 1(a), green rhombus) displays a magnetization of 4.5 emu g⁻¹, which represents a remarkable 40% decrease from the pristine magnetization of 7.5 emu g⁻¹. This same $5 \times 10^{16}~\rm H^+/cm^{-2}$ fluence sample also shows the most dramatic decrease in magnetization, hence the comparison in the magnetization between this compound and the pristine compound will be emphasized for the following discussion of the anisotropic temperature-dependent measurements.

Anisotropic temperature-dependent measurements were also performed along the in-plane direction (H//ab) to gather information about the magnetocrystalline nature of the samples. Figure 2 details a comparison of the H//c (solid symbols) and H//ab (open symbols) magnetization vs. temperature data for both FC (cyan symbols) and ZFC (navy blue symbols) measurements. ZFC measurements were performed by cooling the sample in the absence of a magnetic field. As expected, the magnetization is higher in the H//c direction, as this is the magnetic easy axis of CST and provides clear evidence for a strong perpendicular magnetocrystalline anisotropy in the system [18–26]. This same result is also observed for the irradiated samples, providing evidence that the easy axis remains stable despite a decrease in the magnetization. The H//c measurement for the irradiated sample (figure 2(b)) shows a large bifurcation between the FC and ZFC curves at low temperatures (T < 30 K) that is not present in the pristine magnetization (figure 2(a)), suggesting alterations to the magnetic anisotropy of irradiated CST, potentially due to the change in the magnetic exchange coupling upon proton radiation [27– 30]. In contrast, the H/lab magnetization data is similar in both samples, indicating that the applied field is too small to accurately detect any anisotropic effects in this direction, although this observation may also be due to the spin glass behavior.

Figure 3 shows the isothermal magnetic field-dependent magnetization at all proton fluences as a function of temperatures that are both below (figures 3(a)-(d)) and above (figures 3(e) and (f)) $T_{\rm C}$ (~36 K). Samples were cooled from room temperature to the target measurement temperature and then allowed to reach equilibrium in the absence of a magnetic field. For these measurements, the samples were subjected to a 5-quadrant field sweep, where the field is ramped up from 0 Oe, up to the maximum field of +30 kOe, and then incremented back through 0 Oe and down to -30 kOe, before finally increasing the field back to its maximum value. For isotherms below $T_{\rm C}$, the system is warmed above $T_{\rm C}$ to its paramagnetic state in the absence of a magnetic field upon completing the measurement and cooled to the next target temperature to avoid remanence effects. The measurements were performed in both the H//c (figures 3(a), (c) and (d), solid symbols) and H//ab (figures 3(b), (d) and (f), open symbols) directions, which allows us to qualitatively and quantitatively analyze the magnetocrystalline anisotropy of irradiated CST. From these data, we also extract information regarding the effect of proton irradiation on the saturation magnetization and coercivity of

The magnetization vs magnetic field curves presented in figures 3(a)–(d) offer clear proof of the ferromagnetic phase of CST at temperatures below $T_{\rm C}$. Even after irradiation, all the samples exhibit typical ferromagnetic behavior. We also observe negligible coercivity at all proton fluences. In comparison to the H/lab data (figure 3(b)), the H/lc saturation field is markedly lower, and this provided additional evidence in support of CST maintaining its perpendicular magnetic anisotropy with an H/lc easy axis. Conversely, the H/lab magnetization saturates only at higher fields and shows a more

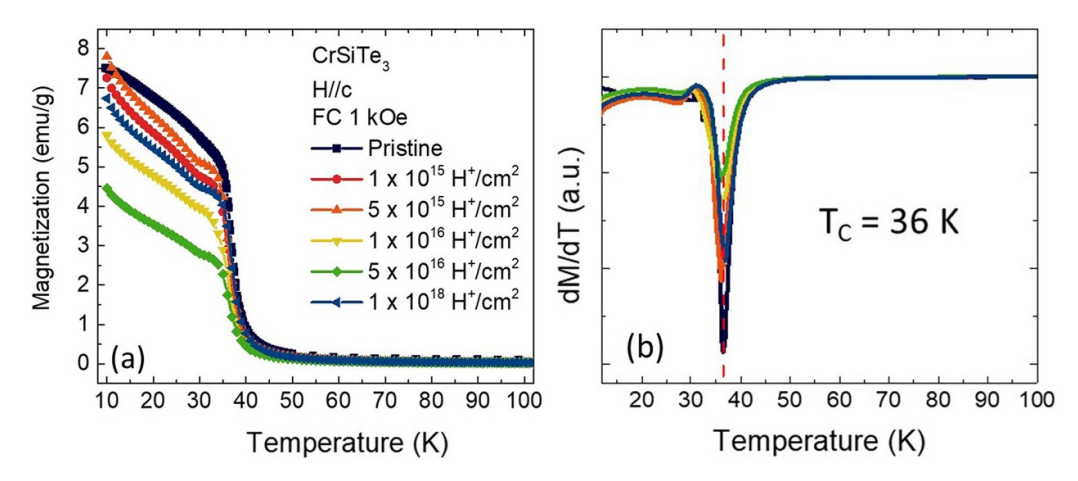


Figure 1. Magnetization vs. temperature (a) and dM/dT vs. temperature (b) shown as a function of fluence showing the ferromagnetic to paramagnetic transition at $T_c = 36$ K for all samples. To note, the magnetization in the ferromagnetic phase is strongly dependent on the proton fluence, whereas, the magnetization is independent of the proton fluence in the paramagnetic phase.

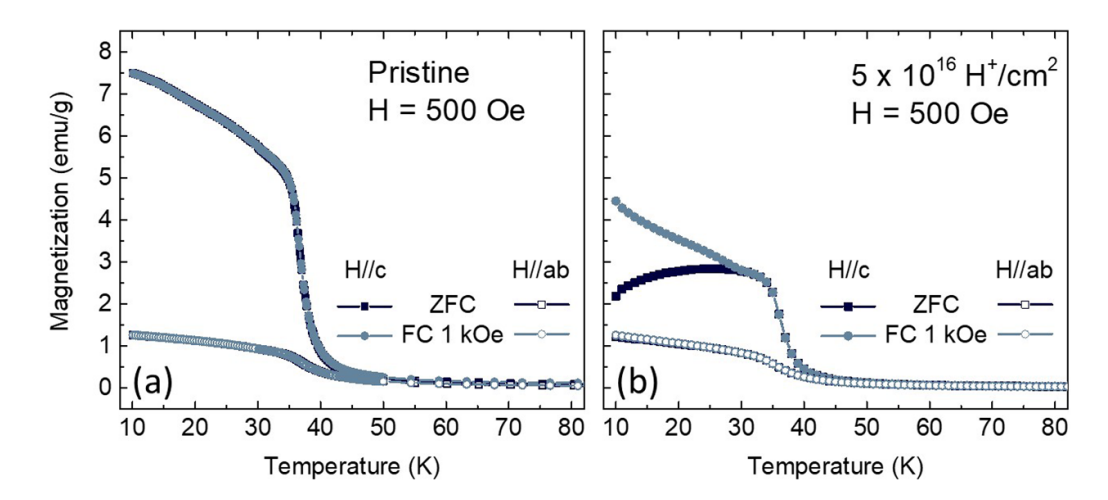


Figure 2. Anisotropic magnetization vs. temperature for both pristine (a) and irradiated (b) CST as a function of cooling field.

gradual onset of saturation. The most obvious change that occurs after irradiation is a reduction in the saturation magnetization, which likely derives from changes in interlayer magnetic exchange coupling in portions of the material, *vide infra*.

Regarding the $5 \times 10^{16} \ H^+/cm^{-2}$ fluence data, the field-dependent magnetization decreases by over 30% compared to the pristine sample, and this observation corroborates the results of the temperature-dependent magnetization measurements. Figure 4 shows the saturation magnetization $M_{\rm sat}$ for all fluences as a function of temperature. The values of $M_{\rm sat}$ are taken from the H//c hysteresis curves at the maximum field. Remarkably, this plot reveals that the reduction in magnetization is not proportional to the number of protons per unit area. In fact, the median fluence of $1 \times 10^{16} \ H^+/cm^{-2}$ (yellow, down triangle) shows lower values of magnetization than the highest fluence of $1 \times 10^{18} \ H^+/cm^{-2}$ (blue, left triangle). Moreover, at a fluence of $5 \times 10^{16} \ H^+/cm^{-2}$, the data shows

the lowest magnetization despite the sample not being subjected to the highest proton fluence. Remarkably, we observe a non-monotonic relationship between the proton fluence and the magnetization (figure 4(a)). As a result, we cannot simply attribute the decrease in magnetization to a destruction of the crystal since the 1×10^{18} H⁺/cm⁻² data would exhibit the lowest magnetization [6–9]. Furthermore, the observed trend persists through the ferromagnetic to paramagnetic transition (figure 4(b)).

We will now focus on the uniaxial anisotropy as a function of proton fluence. It is unlikely that damage to the CST crystals from increased proton irradiation is responsible for the observed reduction in magnetization because the trend between proton fluence and reduced magnetization is not proportional. Therefore, we examined the interatomic interaction of CST by investigating the changes in the magnetocrystalline anisotropy as a function of temperature and proton irradiation fluence. Here, we extracted the effective anisotropy constant,

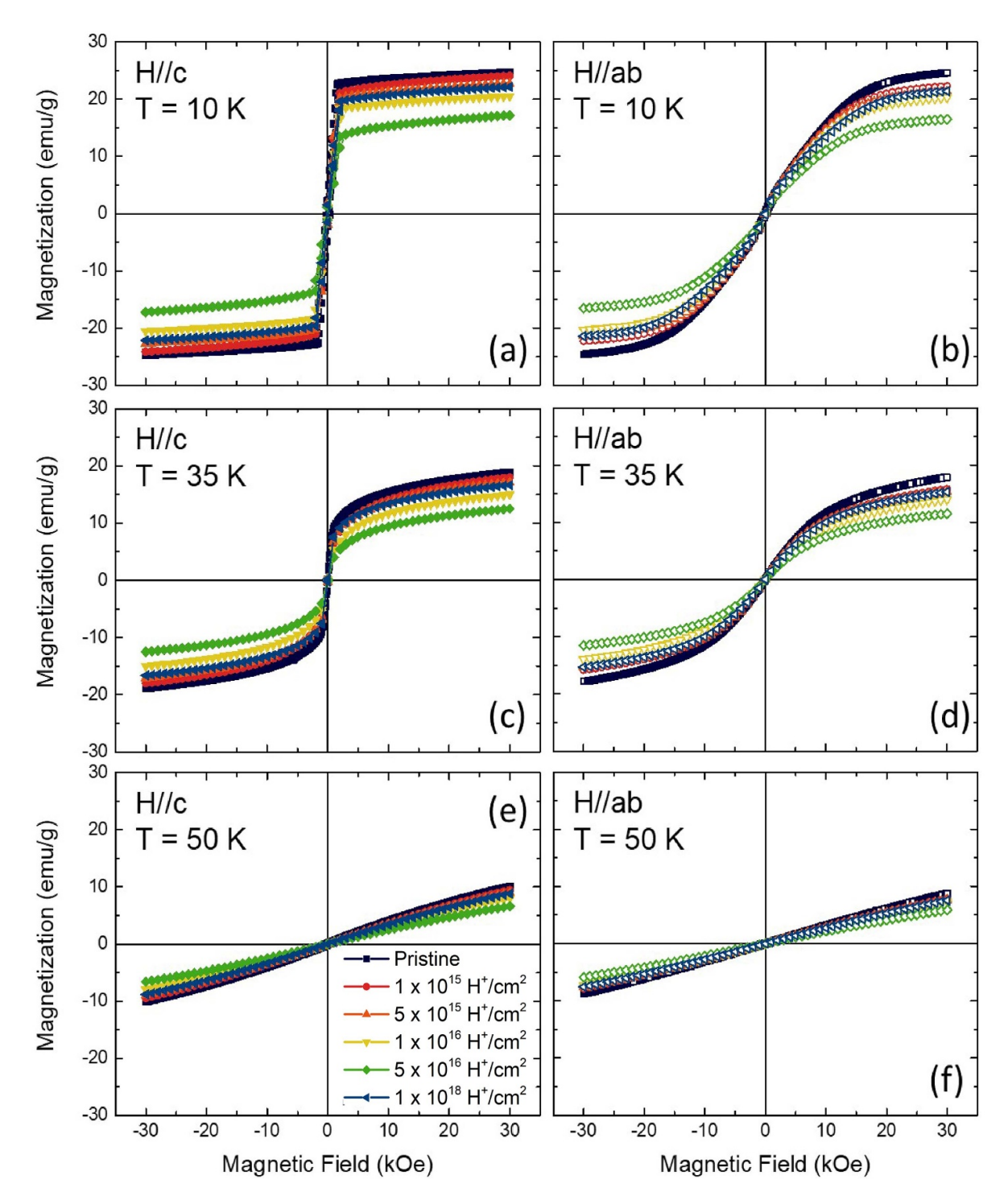


Figure 3. Magnetization vs. magnetic field as a function of fluence for H//c (a), (c), (e) and H//ab (b), (d), (f) at T = 10 K (a), (b), 35 K (c), (d), and 50 K (e), (f).

 $K_{\rm u}$, using the Stoner-Wohlfarth model shown in equation (1) [14, 18, 31–33]:

$$\frac{2K_{\rm u}}{M_{\rm sat}} = \mu_0 H_{\rm sat}.\tag{1}$$

Here, $M_{\rm sat}$ is the saturation magnetization, $H_{\rm sat}$ is the anisotropy field (i.e. the saturation field along the hard axis), and μ_0

is the vacuum permeability. For clarity, the anisotropy field and the saturation magnetization are extracted from magnetic field vs. magnetization measurements performed in the *Hllab* direction. This allowed us to determine the magnitude of the magnetic field necessary to completely align the moments along an unpreferable direction. To estimate the onset of saturation along this direction, the second derivative of the first quadrant magnetization was taken with respect to the magnetic

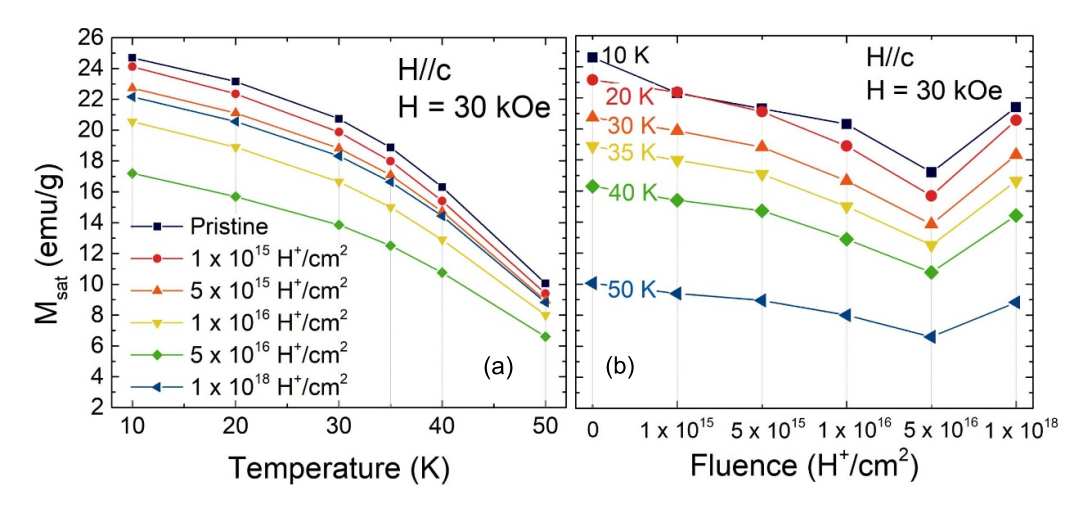


Figure 4. Saturation magnetization M_{sat} vs. temperature as a function of fluence (a) and M_{sat} vs. fluence at each temperature (b) showing non-monotonic relation between magnetization and proton irradiation.

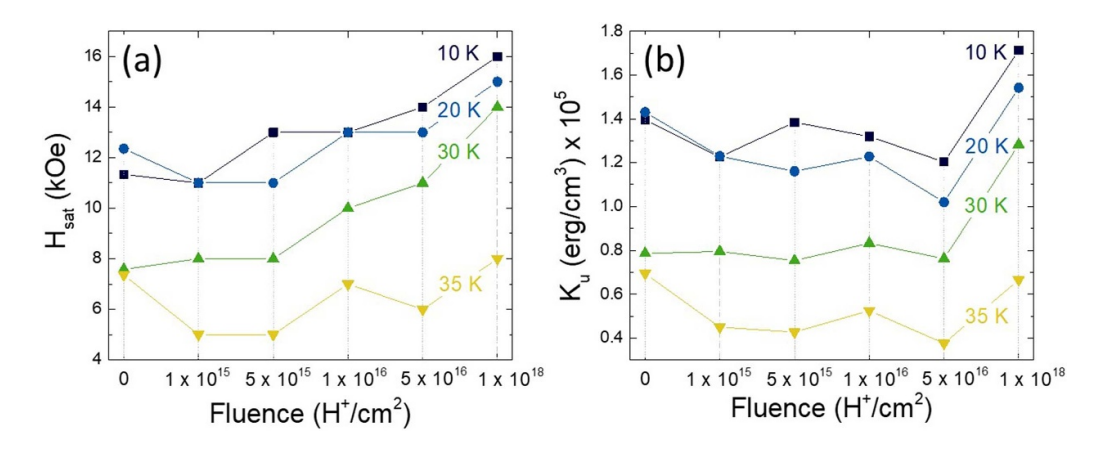


Figure 5. Anisotropy field H_{sat} (a) and uniaxial anisotropy constant K_{u} (b) vs. fluence as a function of temperature.

field and the field magnitude at the local minimum was taken as the saturation/anisotropy field. The multiplicative factor μ_0 is simply unity in cgs units. The values of $H_{\rm sat}$ (figure 5(a)) and $K_{\rm u}$ (figure 5(b)) for pristine CST acquired from this estimation agree well with literature values [26]. In figure 5(b), $K_{\rm u}$ is shown for all fluences as a function of temperature below $T_{\rm C}$. Only temperatures below $T_{\rm C}$ are selected as saturation is not achieved in the paramagnetic region. As expected, the overall values decrease with increasing temperature, but the fluence dependent behavior at each temperature closely mirrors that of the saturation magnetization with no simple linear relation between the two.

The anisotropy constant for the sample irradiated with $5 \times 10^{16} \, \mathrm{H^+/cm^{-2}}$ is consistently lower than that of the other proton fluences across all temperatures. Initially, it appears that this could be due to both a reduced $H_{\rm sat}$ and $M_{\rm sat}$, but a closer inspection of the former reveals a deeper phenomenon related to the temperature dependence of the anisotropy. In fact, a temperature-dependent $H_{\rm sat}$ is direct evidence of a temperature-dependent anisotropic behavior in CST [32, 33]. Moreover, the anisotropy field shows a slight proportionality with the proton fluence. As shown in figure 5(b), we observe that samples irradiated with more protons per unit area

generally require a higher H/lab field to achieve saturation. This trend can be observed more clearly at 20 K (figure 5(a), blue circles), with deviations at other temperatures likely resulting from measurement error.

We observe a decrease in $K_{\rm u}$ for all fluences as the temperature is increased. This phenomenon has been documented in other vdW compounds such as CrI3 and Fe3GeTe2 and is attributed to fluctuating local spin clusters around a macroscopic magnetization vector [18, 32, 33]. Hence, a lower value for $K_{\rm u}$ in the irradiated samples might indicate an effect on the short-range interactions in this material, which could result from the introduction of defects sites that have been created by the proton irradiation. The CST anisotropy is stabilized by two factors, with the first being a slight distortion of the Te octahedra along the c-axis. The second factor is the Te p spin-orbit coupling through the dominant superexchange pathway in CST [22, 23, 34, 35]. This intralyer Cr-Te-Cr superexchange interaction is ferromagnetic, in agreement with the Goodenough-Kanamori rules, and dominates over the weak antiferromagnetic Cr3+ direct exchange interaction, the non-negligible interlayer interactions, and the 2nd and 3rd nearest neighbor intralayer interactions [36]. Therefore, changes in the anisotropy constant could be indirect evidence of modifications to the superexchange interactions present in proton irradiated CST, since it has been reported that the anisotropy of CST is sensitive to changes in both the superexchange interaction and electron–electron repulsions [34]. In addition, though the 2nd and 3rd nearest neighbor interactions represent a superexchange pathway across two Te ligand atoms (Cr–Te–Te–Cr), they present a suitable environment for modifying the interlayer exchange coupling in CST [23, 34]. If this exchange interaction is modified through proton irradiation via interlayer proton enhanced Te–Te coupling, new interlayer antiferromagnetic exchange interactions could account for the reduction in magnetization despite the $T_{\rm C}$ value remaining unchanged.

To shed additional light, we performed extensive temperature dependent X-band EPR measurements on all the proton-irradiated samples along with that of pristine sample. As shown in the supplementary information (see, figures S2–S4 in supplementary information and the related discussion), our initial analysis did not result a conclusive evidence for the observed changes in the magnetic properties upon proton irradiation. However, additional investigations (such as very high frequency EPR etc) are underway to broaden our current understanding on the observed properties.

4. Conclusions and outlook

Exfoliable CST crystals show the versatility of the magnetic properties of vdW compounds upon proton irradiation as a function of proton irradiation. In this study, CST crystals irradiated with up to $1 \times 10^{18} \text{ H}^+/\text{cm}^{-2}$ were studied in a variety of temperature and magnetic field ranges. Through temperature and magnetic field-dependent magnetization, we observe a ferromagnetic phase below $T_{\rm C}\sim36$ K for all fluences. Though the $T_{\rm C}$ remains unchanged after proton irradiation, the saturation magnetization is decreased. Further analysis on the magnetic anisotropy of CST shows a temperature and fluence dependent effect, which could indicate variations in the exchange mechanisms of CST. While further investigations are required, we speculate that the reduced magnetization and uniaxial anisotropy could be a result of reformed short-range intralayer interactions involving the 1st, 2nd, and 3rd nearest neighbor interactions and the interlayer exchange.

Overall, the case of proton irradiated CST presents an exciting environment to not only probe the origin of ferromagnetism in CST and other related compounds, but also to explore other avenues of tuning their magnetic properties for nanoscale magnetic devices and spintronic applications. In effect, proton irradiation could be used to tune the magnetic properties and magnetic interactions of exfoliable vdW materials with tremendous implications for information technology and space exploration.

Data availability statement

All data that support the findings of this study are included within the article (and any supplementary files).

Acknowledgments

This material is based upon work supported by the National Science Foundation Graduate Research Fellowship Program under Grant No. 184874.1 Any opinions, findings, and conclusions or recommendations expressed in this material are those of the author(s) and do not necessarily reflect the views of the National Science Foundation. S R S and H I acknowledge support from the NSF-DMR (Award No. 2105109). SRS acknowledges support from NSF-MRI (Award No. 2018067). M L K acknowledge financial support from the National Science Foundation (MRI Grant CHE-1828744 and Grant CHE-1900237). L M M acknowledges the useful discussions with H S Nair. L M M and S R S acknowledge support from a UTEP start-up grant. L M M acknowledges the Wiemer Family for awarding Student Endowment for Excellence, and NSF-LSAMP PhD. Fellowship. This publication was prepared by S R Singamaneni and co-authors under the Award Number 31310018M0019 from The University of Texas at El Paso (UTEP), Nuclear Regulatory Commission. The Statements, findings, conclusions, and recommendations are those of the author(s) and do not necessarily reflect the view of the (UTEP) or The US Nuclear Regulatory Commission. Work at Brookhaven National Laboratory is supported by the U.S. DOE under Contract No. DESC0012704 (materials synthesis). We note that this work is a part of MS Thesis awarded to Hector Iturraiaga [37].

ORCID iDs

Ju Chen https://orcid.org/0000-0002-5637-7224
Martin Kirk https://orcid.org/0000-0002-1479-3318
Srinivasa R Singamaneni https://orcid.org/0000-0003-1653-9759

References

- [1] Wang Q H *et al* 2022 The magnetic genome of two-dimensional van der Waals materials *ACS Nano* **16** 6960
- [2] Li H, Ruan S and Zeng Y-J 2019 Intrinsic van der Waals magnetic materials from bulk to the 2D limit: new frontiers of spintronics Adv. Mater. 31 1900065
- [3] Jiang X, Liu Q, Xing J, Liu N, Guo Y, Liu Z and Zhao J 2021 Recent progress on 2D magnets: fundamental mechanism, structural design and modification Appl. Phys. Rev. 8 031305
- [4] Mak K F, Shan J and Ralph D C 2019 Probing and controlling magnetic states in 2D layered magnetic materials *Nat. Rev.* Phys. 1 646
- [5] Dayen J-F, Ray S J, Karis O, Vera-Marun I J and Kamalakar M V 2020 Two-dimensional van Der Waals spinterfaces and magnetic-interfaces Appl. Phys. Rev. 7 011303
 - Shultz D A and Kirk M L 2014 Molecular spintronics: a web themed issue *Chem. Commun.* **50** 7401
- [6] Martinez L M, Iturriaga H, Olmos R, Shao L, Liu Y, Mai T T, Petrovic C, Hight Walker A R and Singamaneni S R 2020 Enhanced magnetization in proton irradiated Mn₃Si₂Te₆ van Der Waals crystals Appl. Phys. Lett. 116 172404

- [7] Olmos R, Delgado J A, Iturriaga H, Martinez L M, Saiz C L, Shao L, Liu Y, Petrovic C and Singamaneni S R 2021 Critical phenomena of the layered ferrimagnet Mn₃Si₂Te₆ following proton irradiation *J. Appl. Phys.* 130 013902
- [8] Olmos R, Cosio A, Saiz C L, Martinez L M, Shao L, Wang Q and Singamaneni S R 2019 Magnetic properties of proton irradiated Fe_{2.7}GeTe₂ Bulk Crystals, MRS Adv. 4 2185
- [9] Martinez L M, Saiz C L, Cosio A, Olmos R, Iturriaga H, Shao L and Singamaneni S R 2019 Magnetic properties of proton irradiated Mn₃Si₂Te₆ van der Waals single crystals MRS Adv. 4 2177
- [10] Shi T, Peng Q, Bai Z, Gao F and Jovanovic I 2019 Proton irradiation of graphene: insights from atomistic modeling *Nanoscale* 11 20754
- [11] Yazyev O V 2008 Magnetism in disordered graphene and irradiated graphite *Phys. Rev. Lett.* **101** 037203
- [12] Zhang C et al 2021 Pressure-enhanced ferromagnetism in layered CrSiTe₃ flakes Nano Lett. 21 7946
- [13] Li Y, Chen Z, Wang J, li T, Tian M, Karel J and Suzuki K 2023 Abnormal thickness-dependent magneto-transport properties of vdW magnetic semiconductor Cr₂Si₂Te₆ npj 2D Mater. Appl. 7 39
- [14] Zhang C et al 2022 Hard ferromagnetic behavior in atomically thin CrSiTe₃ flakes Nanoscale 14 5851
- [15] Walker R C, Shi T, Silva E C, Jovanovic I and Robinson J A 2016 Phys. Status Solidi A 213 3065
- [16] Krasheninnikov A V and Nordlund K 2010 J. Appl. Phys. 107 071301
- [17] Geremew A et al 2019 arXiv:1901.00551
- [18] Liu Y and Petrovic C 2019 Anisotropic magnetic entropy change in Cr₂X₂Te₆ (X = Si and Ge) *Phys. Rev. Mater.* 3 014001
- [19] Carteaux V, Ouvrard G, Grenier J C and Laligant Y 1991 Magnetic structure of the new layered ferromagnetic chromium hexatellurosilicate Cr₂Si₂Te₆ J. Magn. Magn. Mater. 94 127
- [20] Siberchicot B, Jobic S, Carteaux V, Gressier P and Ouvrard G 1996 Band structure calculations of ferromagnetic chromium tellurides CrSiTe₃ and CrGeTe₃ J. Phys. Chem. 100 5863
- [21] Liu B, Zou Y, Zhang L, Zhou S, Wang Z, Wang W, Qu Z and Zhang Y 2016 Critical behavior of the quasi-two-dimensional semiconducting ferromagnet CrSiTe₃ Sci. Rep. 6 1
- [22] Zhang J et al 2019 Unveiling electronic correlation and the ferromagnetic superexchange mechanism in the van der Waals crystal CrSiTe₃ Phys. Rev. Lett. 123 047203
- [23] Williams T J, Aczel A A, Lumsden M D, Nagler S E, Stone M B, Yan J-Q and Mandrus D 2015 Magnetic

- correlations in the quasi-two-dimensional semiconducting ferromagnet CrSiTe₃ *Phys. Rev.* B **92** 144404
- [24] Casto L D et al 2015 Strong spin-lattice coupling in CrSiTe₃ APL Mater. 3 041515
- [25] Wu S, Wang L, Gao B, Wang Y, Oh Y S, Cheong S-W, Hong J and Wang X 2018 The direct observation of ferromagnetic domain of single crystal CrSiTe₃ AIP Adv. 8 055016
- [26] Niu W, Zhang X, Wang W, Sun J, Xu Y, He L, Liu W and Pu Y 2021 Probing the atomic-scale ferromagnetism in van der Waals Magnet CrSiTe₃ Appl. Phys. Lett. 119 172402
- [27] Long F et al 2023 Ferromagnetic interlayer coupling in CrSBr crystals irradiated by ions Nano Lett. 23 8468
- [28] Mahendraa A, Guptab P, Granville S and Kennedy J 2022 Tailoring of magnetic anisotropy by ion irradiation for magnetic tunnel junction sensors J. Alloys Compd. 910 164902
- [29] Makarova T L, Shelankov A L, Serenkov I T, Sakharov V I and Boukhvalov D W 2011 Anisotropic magnetism of graphite irradiated with medium-energy hydrogen and helium ions *Phys. Rev.* B 83 085417
- [30] Yuan Y et al 2018 Switching the uniaxial magnetic anisotropy by ion irradiation induced compensation J. Phys. D: Appl. Phys. 51 145001
- [31] Stoner E C and Wohlfarth E P 1948 A mechanism of magnetic hysteresis in heterogeneous alloys *Phil. Trans. R. Soc.* A **240** 599-642
- [32] Richter N, Weber D, Martin F, Singh N, Schwingenschlögl U, Lotsch B V and Kläui M 2018 Temperature-dependent magnetic anisotropy in the layered magnetic semiconductors CrI₃ and CrBr₃ Phys. Rev. Mater. 2 024004
- [33] Liu Y, Li J, Tao J, Zhu Y and Petrovic C 2019 Anisotropic magnetocaloric effect in Fe_{3-x}GeTe₂ Sci. Rep. 9 13233
- [34] Sivadas N, Daniels M W, Swendsen R H, Okamoto S and Xiao D 2015 Magnetic ground state of semiconducting transition-metal trichalcogenide monolayers *Phys. Rev.* B 91 235425
- [35] Kim D-H, Kim K, Ko K-T, Seo J, Kim J S, Jang T-H, Kim Y, Kim J-Y, Cheong S-W and Park J-H 2019 Giant magnetic anisotropy induced by ligand L S coupling in layered Cr compounds *Phys. Rev. Lett.* 122 207201
- [36] Hatfield W E 1976 Properties of condensed compounds (compounds with spin exchange) Theory and Applications of Molecular Paramagnetism ed E A Boudreaux and L N Mulay (Wiley Interscience) ch 7, pp 381–5
- [37] Iturriaga H 2022 Exploring tunable magnetization and high-temperature ferromagnetism in ternary transition metal-based chalcogenides *MS Thesis* (The University of Texas at El Paso (UTEP)